Mobile Networks and Applications
https://doi.org/10.1007/s11036-021-01756-y

Evaluating the Performance of Full-Duplex Energy Harvesting Vehicle-to-Vehicle Communication System over Double Rayleigh Fading Channels

Ba Cao Nguyen[1] · Tran Manh Hoang[1] · Xuan Nam Tran[2] · Xuan Nghia Pham[2] · Le The Dung[3,4]

Accepted: 2 June 2020

Abstract

In this paper, we analyze the performance of vehicle-to-vehicle (V2V) communication system, which employs full-duplex (FD) and energy harvesting (EH) techniques at source and relay nodes from power beacon (PB) through radio frequency. Unlike previous systems where all nodes located at fixed locations, we investigate the case that three nodes (source, relay, and destination) are moving vehicles. Therefore, the channels between them follow double (cascade) Rayleigh fading distributions. Furthermore, the source and relay nodes can harvest the energy from PB for data transmission when they move on the road. We derive the exact expressions of the outage probability (OP) and symbol error probability (SEP) of the proposed system and then intensively study the impacts of various parameters such as the number transmission antennas of PB, the time duration for EH, the distances between nodes, and the residual self-interference (RSI) at the FD relay node on the system performance. Monte-Carlo simulations validate all theory analysis. Numerical results show that system performance is strongly impacted by the number of transmission antennas of the power beacon, the EH duration, the RSI, and the distances between nodes. Moreover, for a given transmission of power beacon and the SIC capability of the FD relay node, there exist optimal EH duration and optimal distance from the source to relay, which provide the best system performance.

Keywords Vehicle-to-vehicle communication · Full-duplex · Energy harvesting · Self-interference cancellation · Outage probability · Symbol error probability

✉ Le The Dung
lethedung@tdtu.edu.vn

Ba Cao Nguyen
nguyenbacao@tcu.edu.vn

Tran Manh Hoang
tranmanhhoang@tcu.edu.vn

Xuan Nam Tran
namtx@mta.edu.vn

Xuan Nghia Pham
nghiapx@mta.edu.vn

[1] Telecommunications University, Khanh Hoa, Vietnam

[2] Le Quy Don Technical University, Hanoi, Vietnam

[3] Divison of Computational Physics, Institute for Computational Science, Ton Duc Thang University, Ho Chi Minh City, Vietnam

[4] Faculty of Electrical and Electronics Engineering, Ton Duc Thang University, Ho Chi Minh City, Vietnam

1 Introduction

Nowadays, most people in the world use smart devices. Unlike the previous decade, when regular cell phones were used; today, smartphones are not only used for voice but also for many other functions such as exchanging the information to control many things, especially in the age of the Internet of Things (IoT). Hence, improving the spectrum efficiency to support the increasing demand for future wireless networks becomes an urgent mission. To deploy the fifth-generation (5G) mobile communication systems around 2020, various technologies such as full-duplex (FD), massive multiple-input multiple-output (MIMO), non-orthogonal multiple access (NOMA) [1–4] are researched and experimented. Among those solutions, FD technology is very promising because the FD devices can transmit and receive signals at the same time and on the same frequency band simultaneously, thus can theoretically double the spectral efficiency and capacity [5–11]. However, self-interference (SI) from the transmission antenna to receiving

Published online: 01 May 2021

antenna of the FD devices is a big problem for FD communication systems. Fortunately, through using new techniques in antenna design, analog, and digital processing, the FD devices can suppress SI up to 110 dB which makes the FD communication becomes more realistic [12–14].

Recently, the FD technique is not only able to double the spectral efficiency but also has other advantages such as reducing the feedback and end-to-end delay, improving the network secrecy and the effectiveness of ad hoc network protocols, enhancing the spectrum usage flexibility and the system throughput, collision avoidance, solving the hidden terminal problem, and reducing congestion through the aid of Medium Access Layer (MAC) scheduling [1]. Therefore, the usage of the FD technique in wireless communication systems has attracted much attention in both education and industry [10]. Especially, employing the FD technique at relay nodes to increase the coverage and reliability of the wireless system is considered as a promising solution [15–19].

Today, smart devices are often mobile and connect to other devices for data exchange, and form the device-to-device (D2D) or vehicle-to-vehicle (V2V) communications. In [3, 20–24], the V2V communication systems have been investigated and analyzed. In [20], the advantages of V2V communication such as safety applications, direct D2D/V2V are considered. The authors indicated that V2V communication is the crucial key for cooperative and semi-autonomous driving. The ergodic capacity of the V2V communication system over Rician fading channels was investigated in [3, 21]. The authors derived the approximate expression of the average capacity and simulated the bit error rate (BER) of the system. Their results demonstrated that using NOMA in the V2V system can improve the reliability of communication link and bandwidth efficiency.

Due to the applications of both FD technique and V2V communication in 5G and next-generation systems, combining the FD and V2V communication in these systems has been considered in many works [3, 20, 22, 23] because FD technique can reduce the end-to-end delay of communication links between vehicles. Besides analyzing the performance of the FD-V2V system, many solutions such as antenna design [22], interference management [23] have been introduced to enhance the self-interference cancellation, which then improves the performance and capacity of the system because of the reduction in the SI. In [22], the authors proposed a dual-band full-duplex antenna/array, which can be applied in intelligent transport systems (ITS). By combining multiple functions in a device, the size, weight, and cost of an antenna can be reduced. In [23], the FD vehicular access network was considered in the case of imperfect channel state information (CSI) at the transmitter. An optimal blind interference alignment scheme was proposed to improve the sum rate of the system.

It is easy to see from the above discussions that the usage of the FD technique in the V2V communication system is vitally necessary for reducing the transmission delay and improving the spectrum efficiency. However, when wireless devices move on the road and exchange the information for a long time, it is difficult to supply power to them. Thus, to maintain the connectivity to the other devices, the moving wireless devices need to harvest the energy from the radio frequency (RF) signals and then use this harvested energy for the data transmission. On the other hand, the energy harvesting (EH) technique is a promising method for V2V communication systems thanks to the advantages of wireless charging. Moreover, the combination of EH and new technologies for wireless communication systems such as FD and NOMA becomes a hot topic [5, 10, 16, 28–31]. In these studies, the authors demonstrated that those systems could be deployed in realistic scenarios when various self-interference cancellation (SIC) is applied.

Meanwhile, although the EH technique is a crucial key for wireless devices in the V2V communication systems, there is a lack of research on the EH-V2V systems because the harvested energy of the wireless devices is small and depends on the instantaneous channel gain of the RF signal. On the other hand, in V2V communication systems, the channels between vehicles are usually considered as double Rayleigh fading channels, which are worse than Rayleigh fading channels [25, 26]. Furthermore, it is hard to derive the closed-form expression of OP and SEP because many instantaneous channel gains appear. Despite these issues, combining EH and FD into a V2V system is considered as an inevitable trend for future wireless networks. It is because FD can significantly reduce the delay in V2V communication systems compared with traditional half-duplex (HD) mode by sensing the environment and sending information simultaneously. Additionally, the usage of EH at the transmitters can solve the problem of limited-energy vehicles, especially when it is hard to supply power for the transmitters, specifically when EH is exploited by the dedicated power from power beacon (PB). Furthermore, the large space on the rooftop of vehicle provides a good isolation between the transmission and reception antennas of FD node, thus, improving system performance because the SIC capability is better.

Motivated by the above discussions, in this paper, we investigate an EH-FD-V2V relay system, where the source node transmits signals to the destination node through the assistance of the relay node. In this system, source, relay, and destination nodes move on the road while they transmit and receive signals. Furthermore, the relay node operates in FD mode. Due to the long transmission time, the source and relay nodes must harvest energy from a PB and then use the harvested energy to support the data transmission. So far, this is the first work that combines both EH and

FD techniques in a V2V communication system. Based on the mathematical calculations, we successfully derived the exact expressions of OP and SEP of the proposed system. The contributions of this paper can be summarized as follows:

- We consider a V2V system where the source and the FD relay nodes harvest energy from power beacon through RF before transmitting signal. To increase the harvested energy at source and relay nodes, we investigate the case that the power beacon has multiple transmission antennas.
- We derive the exact closed-form mathematical expressions for the OP and SEP of the proposed system over double Rayleigh fading channels and under the impact of residual self-interference (RSI) which is caused by the imperfect SIC. Furthermore, we also investigate the system throughput.
- We find that the system performance is strongly impacted by the number of transmission antennas of the power beacon, the EH duration, the RSI, and the distances between nodes. Moreover, for a given transmission of power beacon and the SIC capability of the FD relay node, there exist optimal EH duration and optimal distance from the source to relay, which provide the best system performance. All analysis results are validated through Monte-Carlo simulations.

The rest of this paper is organized as follows. We present the system model of the proposed EH-FD-V2V relay system in Section 2 and then derive the system performance in terms of the OP and SEP in Section 3. In Section 4, we provide numerical results and discussions. Finally, we conclude our paper in Section 5.

2 System model

The system model of the proposed EH-FD-V2V relay system is illustrated in Fig. 1. There are four nodes in this system, i.e., a power beacon (PB), a source node (S), a relay node (R), and a destination node (D). The data transmission from S to D is assisted by R. In the proposed system, S is a device which has one antenna for both harvesting energy and transmitting signal. D has an antenna for receiving signal. S and D operate in half-duplex (HD) mode, while R operates in FD mode with two antennas, one for transmitting and another for receiving. Furthermore, since S, R and D move on the road and exchange the information for a long time, the portable power supplies of S and R are insufficient. To address this problem, S and R need to harvest the radio frequency (RF) energy from PB first and then exchange data.

In our work, we consider the case that S and R have suitable circuits to harvest the energy and have superior capacitors to store the harvested energy. Moreover, S and R fully use the harvested energy for transmitting signals in one symbol period. To increase the amount of harvested energy at S and R, we assume that PB has K transmission antennas and the average transmission power P is equal for all antennas of PB. Generally, there are two EH protocols commonly used in wireless systems, i.e., time switching (TS) and power splitting (PS) protocols. The combination of these two protocols has also been applied in various works to increase the amount of harvested energy. In this paper, we use TS protocol because it is can be deployed more easily than the PS protocol in practice. The operation of the proposed EH-FD-V2V relay system using TS protocol consists of two stages, as shown in Fig. 2. We denote $\mathcal{T}$ as the time duration of the entire transmission block. In the first stage, S and R harvest the RF energy from PB. The time duration of the first stage is $\alpha\mathcal{T}$, where α, $0 \leqslant \alpha \leqslant 1$, represents the time switching ratio. In the second stage, S and R use the harvested energy for transmitting and receiving signals. The time duration for the second stage is $(1-\alpha)\mathcal{T}$. Since R receives signals from S and transmits these signals to D at the same time, the self-interference occurs.

For the EH duration $\alpha\mathcal{T}$, the harvested energy at S (denoted by E_h^{S}) and R (denoted by E_h^{R}) can be calculated as [38]

$$E_h^{\mathrm{S}} = \eta\alpha\mathcal{T}P\sum_{i=1}^{\mathrm{K}}|h_{i\mathrm{S}}|^2, \tag{1}$$

$$E_h^{\mathrm{R}} = \eta\alpha\mathcal{T}P\sum_{i=1}^{\mathrm{K}}|h_{i\mathrm{R}}|^2, \tag{2}$$

where η is the energy conversion efficiency. For given circuit, the energy conversion efficiency is a constant and its value depends on the rectification process and the EH circuitry ($0 \leqslant \eta \leqslant 1$); P is the average transmission power at an antenna of PB; $h_{i\mathrm{S}}$ and $h_{i\mathrm{R}}$ are the fading coefficients from ith antenna of PB to S and R, respectively. It is noted that E_h^{R} in Eq. 2 can be increased when both antennas of R are used for harvesting energy. However, the transmission power of R will also be increased, leading to higher SI at R which may reduce the system performance [27]. Therefore, in this paper, we consider the case that R only uses one antenna for EH. After converting the harvested energy, the transmission power of S and R can be calculated as [32]

$$P_{\mathrm{S}} = \frac{\eta\alpha\mathcal{T}P\sum\limits_{i=1}^{\mathrm{K}}|h_{i\mathrm{S}}|^2}{(1-\alpha)\mathcal{T}} = \frac{\eta\alpha P\sum\limits_{i=1}^{\mathrm{K}}|h_{i\mathrm{S}}|^2}{1-\alpha}, \tag{3}$$

$$P_{\mathrm{R}} = \frac{\eta\alpha\mathcal{T}P\sum\limits_{i=1}^{\mathrm{K}}|h_{i\mathrm{R}}|^2}{(1-\alpha)\mathcal{T}} = \frac{\eta\alpha P\sum\limits_{i=1}^{\mathrm{K}}|h_{i\mathrm{R}}|^2}{1-\alpha}. \tag{4}$$

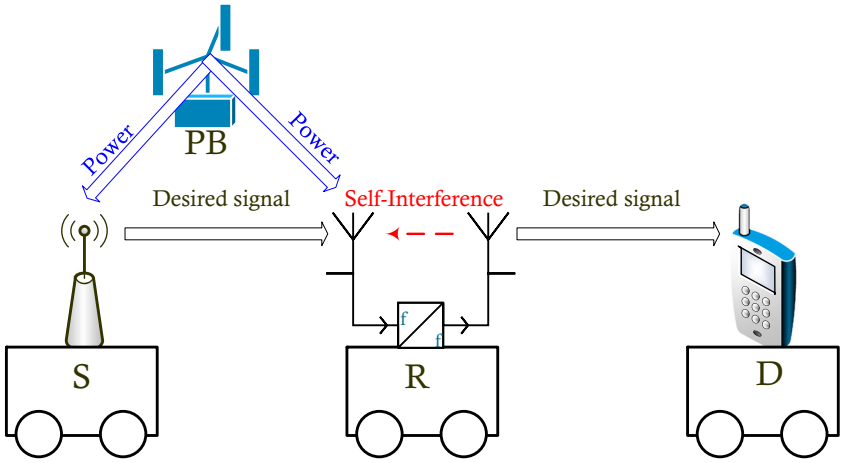

Fig. 1 System model of the proposed EH-FD-V2V relay system

During the time duration $(1-\alpha)\mathcal{T}$ for exchanging information, S transmits signal to R, while R forwards the signal to D at the same time and on the same frequency band. This transmission process may generate the SI at R. Therefore, the received message at R is given by

$$y_{\mathrm{R}} = h_{\mathrm{SR}}\sqrt{d_{\mathrm{SR}}^{-\beta} P_{\mathrm{S}}}x_{\mathrm{S}} + \tilde{h}_{\mathrm{RR}}\sqrt{d_{\mathrm{RR}}^{-\beta} P_{\mathrm{R}}}x_{\mathrm{R}} + n_{\mathrm{R}}, \tag{5}$$

where x_{S} and x_{R} are the transmitted signals at S and R, respectively; d_{SR} and d_{RR} are respectively the distances from S to R and from transmission antenna to reception antenna of R; β is the path loss exponent whose values range from 2 to 6; h_{SR} and $\tilde{h}_{\mathrm{RR}}$ are the fading coefficients of the channels from S to R, and from the transmission antenna to the reception antenna of R, respectively; n_{R} is the Additive White Gaussian Noise (AWGN) with zero-mean and variance σ^2, i.e., $n_{\mathrm{R}} \sim \mathcal{CN}(0, \sigma^2)$.

As can be seen from Eq. 5, the average power of SI at R before doing SIC is calculated as

$$\mathbb{E}\{|\tilde{h}_{\mathrm{RR}}|^2 d_{\mathrm{RR}}^{-\beta} P_{\mathrm{R}}\} = \frac{\eta\alpha P}{1-\alpha}\mathbb{E}\left\{|\tilde{h}_{\mathrm{RR}}|^2 d_{\mathrm{RR}}^{-\beta}\sum_{i=1}^{\mathrm{K}}|h_{i\mathrm{R}}|^2\right\}, \tag{6}$$

where $\mathbb{E}\{.\}$ denotes the expectation operator.

Since the distance between the transmission antenna and the reception antenna of R is very small, the power of SI is much stronger than that of the desired signal. Therefore, in this paper, we assume that R can apply all SIC techniques, such as antenna propagation, analog suppression, and digital cancellation, to enhance the quality of the desired signal. Especially, since R knows its transmitted signal, it can subtract SI from the received signals by using the digital cancellation method [13, 33, 37, 39]. On the other hand, due to the error in estimating the SI channel and the faulty hardware for SIC, the RSI still exists at R. Notably, the RSI at R, denoted by I_{R}, has a complex Gaussian distribution with zero mean and variance γ_{RSI} [11, 13, 34–37, 39]. Moreover, γ_{RSI} is calculated as

$$\gamma_{\mathrm{RSI}} = \tilde{\Omega}\frac{\eta\alpha P}{1-\alpha}, \tag{7}$$

where $\tilde{\Omega}$ represents the SIC capability of the FD device.

After various SIC techniques are applied, Eq. 5 can be rewritten as

$$y_{\mathrm{R}} = h_{\mathrm{SR}}\sqrt{d_{\mathrm{SR}}^{-\beta} P_{\mathrm{S}}}x_{\mathrm{S}} + I_{\mathrm{R}} + n_{\mathrm{R}}, \tag{8}$$

and the received signal at D can be expressed as

$$y_{\mathrm{D}} = h_{\mathrm{RD}}\sqrt{d_{\mathrm{RD}}^{-\beta} P_{\mathrm{R}}}x_{\mathrm{R}} + n_{\mathrm{R}}, \tag{9}$$

where h_{RD} and d_{RD} are respectively the fading coefficient of R − D channel and the distance from R to D; n_{D} is the AWGN at D with zero mean and variance of σ^2, i.e., $n_{\mathrm{D}} \sim \mathcal{CN}(0, \sigma^2)$.

Based on Eqs. 8 and 9, the signal-to-interference-plus-noise ratios (SINRs) at R and D are calculated as

$$\gamma_{\mathrm{R}} = \frac{|h_{\mathrm{SR}}|^2 P_{\mathrm{S}}}{d_{\mathrm{SR}}^{\beta}(\gamma_{\mathrm{RSI}} + \sigma^2)} = \frac{\eta\alpha P|h_{\mathrm{SR}}|^2}{(1-\alpha)d_{\mathrm{SR}}^{\beta}(\gamma_{\mathrm{RSI}} + \sigma^2)}\sum_{i=1}^{\mathrm{K}}|h_{i\mathrm{S}}|^2. \tag{10}$$

$$\gamma_{\mathrm{D}} = \frac{|h_{\mathrm{RD}}|^2 P_{\mathrm{R}}}{d_{\mathrm{RD}}^{\beta}\sigma^2} = \frac{\eta\alpha P|h_{\mathrm{SR}}|^2}{(1-\alpha)d_{\mathrm{RD}}^{\beta}\sigma^2}\sum_{i=1}^{\mathrm{K}}|h_{i\mathrm{R}}|^2. \tag{11}$$

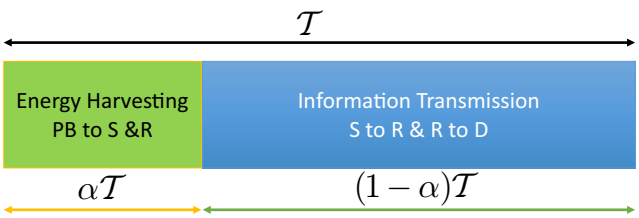

Fig. 2 Time duration for EH and information transmission of the proposed EH-FD-V2V relay system

We note that in wireless relay system which uses DF protocol, the end-to-end SINR is given by

$$\gamma_{\text{e2e}} = \min\{\gamma_{\text{R}}, \gamma_{\text{D}}\}. \tag{12}$$

On the other hand, in the V2V system with double Rayleigh fading channels, the instantaneous channel gain of S − R link is computed by multiplying two independent instantaneous channel gains of Rayleigh fading channels, i.e., $|h_{\text{SR}}|^2 = |h_{\text{SR}_1}|^2|h_{\text{SR}_2}|^2$, where $|h_{\text{SR}_1}|^2$ and $|h_{\text{SR}_2}|^2$ are the instantaneous channel gain of Rayleigh fading channel. Similarly, for R − D link, we have $|h_{\text{RD}}|^2 = |h_{\text{RD}_1}|^2|h_{\text{RD}_2}|^2$.

3 System performance

3.1 Outage probability

The outage probability (OP) of a wireless system is the probability that the instantaneous SINR is less a certain threshold [40]. Let $\mathcal{R}_1$ and $\mathcal{R}_2$ (bit/s/Hz) be the minimum required data rates from S to R and from R to D. For simplicity, we assume that $\mathcal{R}_1 = \mathcal{R}_2 = \mathcal{R}$. Therefore, the OP of the proposed EH-FD-V2V relay system is defined as

$$\begin{aligned} P_{\text{out}} &= \Pr\{(1-\alpha)\log_2(1+\gamma_{\text{e2e}}) < \mathcal{R}\}, \\ &= \Pr\{\gamma_{\text{e2e}} < 2^{\frac{\mathcal{R}}{1-\alpha}} - 1\} = \Pr\{\gamma_{\text{e2e}} < x\}, \end{aligned} \tag{13}$$

where $x = 2^{\frac{\mathcal{R}}{1-\alpha}} - 1$ is the threshold. Substituting Eqs. 12 into 13, we have

$$P_{\text{out}} = \Pr\{\min\{\gamma_{\text{R}}, \gamma_{\text{D}}\} < x\}. \tag{14}$$

Applying the probability law in [41] for two independent random variables, i.e., $\Pr\{\mathcal{A} \cup \mathcal{B}\} = \Pr\{\mathcal{A}\} + \Pr\{\mathcal{B}\} - \Pr\{\mathcal{A}\}\Pr\{\mathcal{B}\}$, where $\mathcal{A}$ and $\mathcal{B}$ are two independent random variables, Eq. 14 can be rewritten as

$$\begin{aligned} P_{\text{out}} &= \Pr\{\gamma_{\text{R}} < x\} + \Pr\{\gamma_{\text{D}} < x\} \\ &\quad -\Pr\{\gamma_{\text{R}} < x\}\Pr\{\gamma_{\text{D}} < x\}. \end{aligned} \tag{15}$$

From Eq. 15, the OP of the proposed EH-FD-V2V relay system is determined in the following Theorem 1.

Theorem 1 *The outage probability of the proposed system under the impact of RSI and double Rayleigh fading distributions is calculated as*

$$\begin{aligned} P_{out} &= 1 - \frac{\pi^2\sqrt{AB}x}{4MN(\Omega_1\Omega_2)^{\text{K}-1}\Gamma^2(\text{K})} \\ &\quad \times \sum_{m=1}^{M}\sum_{n=1}^{N}\sqrt{(1-\phi_m^2)(1-\phi_n^2)}K_1\left(\sqrt{\frac{Ax}{-\Omega_1\ln u}}\right) \\ &\quad \times K_1\left(\sqrt{\frac{Bx}{-\Omega_2\ln v}}\right)(\Omega_1\Omega_2\ln u\ln v)^{\text{K}-\frac{3}{2}}, \end{aligned} \tag{16}$$

where

$$A = \frac{4(1-\alpha)d_{SR}^{\beta}(\gamma_{RSI}+\sigma^2)}{\Omega_3\Omega_4\eta\alpha P}; \; B = \frac{4(1-\alpha)d_{RD}^{\beta}\sigma^2}{\Omega_5\Omega_6\eta\alpha P};$$

$\Omega_1 = \mathbb{E}\{|h_{i\text{S}}|^2\}$; $\Omega_2 = \mathbb{E}\{|h_{iR}|^2\}$; $\Omega_3 = \mathbb{E}\{|h_{SR_1}|^2\}$; $\Omega_4 = \mathbb{E}\{|h_{SR_2}|^2\}$; $\Omega_5 = \mathbb{E}\{|h_{RD_1}|^2\}$; $\Omega_6 = \mathbb{E}\{|h_{RD_2}|^2\}$; *$\Omega_i$ refers to the average channel gain of Rayleigh fading channel, $i = 1, 2, ..., 6$; $\mathbb{E}$ denotes the expectation operator; M and N are the complexity-accuracy trade-off parameter;* $\phi_m = \cos\left(\frac{(2m-1)\pi}{2M}\right)$; $u = \frac{1}{2}(\phi_m+1)$; $\phi_n = \cos\left(\frac{(2n-1)\pi}{2N}\right)$; $v = \frac{1}{2}(\phi_n+1)$; *$K_1(.)$ and $\Gamma(.)$ are respectively the first-order modified Bessel function of the second kind and the Gamma function* [42].

Proof From Eq. 15, we need to compute the probability $\Pr\{\gamma_{\text{R}} < x\}$ and $\Pr\{\gamma_{\text{D}} < x\}$ to achieve (16) in Theorem 1. Firstly, we start with the cumulative distribution function (CDF), and the probability density function (PDF) of the channel gains of Rayleigh fading channels which are respectively given by

$$F_{|h|^2}(x) = 1 - \exp\left(-\frac{x}{\Omega}\right), x \geqslant 0, \tag{17}$$

$$f_{|h|^2}(x) = \frac{1}{\Omega}\exp\left(-\frac{x}{\Omega}\right), x \geqslant 0. \tag{18}$$

For the summation of channel gains, i.e., $X = \sum_{i=1}^{\text{K}}|h|^2$, its CDF and PDF are respectively calculated as [43]

$$F_X(x) = 1 - \exp\left(-\frac{x}{\Omega}\right)\sum_{i=0}^{\text{K}-1}\left(\frac{x}{\Omega}\right)^i, x \geqslant 0, \tag{19}$$

$$f_{|h|^2}(x) = \frac{x^{\text{K}-1}}{\Omega^{\text{K}}\Gamma(\text{K})}\exp\left(-\frac{x}{\Omega}\right), x \geqslant 0. \tag{20}$$

Applying Eqs. 17, 18, 19, and 20, we obtain (A2), and then derive Eqs. A8 and A9. Using Eq. 15, we obtain the OP of the proposed system as in Theorem 1. □

The detailed proof is presented in Appendix A.

3.2 Symbol error probability

For the wireless system, SEP can be calculated as [40]

$$\text{SEP} = a\mathbb{E}\{Q(\sqrt{b\gamma})\} = \frac{a}{\sqrt{2\pi}}\int_0^{\infty}F\left(\frac{t^2}{b}\right)e^{-\frac{t^2}{2}}dt, \tag{21}$$

where $Q(x) = \frac{1}{\sqrt{2\pi}}\int_x^{\infty}e^{-t^2/2}dt$ is the Gaussian function; a and b are certain values that depend on the modulation types [40], i.e., $a = 1, b = 2$ for the binary phase-shift keying

(BPSK) and $a = 2, b = 1$ for the quadrature phase shift keying (QPSK); γ and $F(.)$ are the end-to-end SINR and its CDF, respectively.

From Eq. 21, we obtain the SEP of the proposed system in the following Theorem 2.

Theorem 2 *The SEP of the proposed EH-FD-V2V relay system is calculated as*

$$SEP = \frac{a\sqrt{b}}{2\sqrt{2\pi}}\Bigg[\sqrt{\frac{2\pi}{b}} - \frac{\pi^3\sqrt{AB}}{4MNJb(\Omega_1\Omega_2)^{\mathrm{K}-1}\Gamma^2(\mathrm{K})} \times \sum_{m=1}^{M}\sum_{n=1}^{N}\sum_{j=1}^{J}\sqrt{(1-\phi_m^2)(1-\phi_n^2)(1-\phi_j^2)} \times (\Omega_1\Omega_2 \ln u \ln v)^{\mathrm{K}-\frac{3}{2}}\sqrt{\frac{-2\ln w}{b}} \times K_1\left(\sqrt{\frac{2A\ln w}{b\Omega_1 \ln u}}\right)K_1\left(\sqrt{\frac{2B\ln w}{b\Omega_2 \ln v}}\right), \quad (22)$$

where J is the complexity-accuracy trade-off parameter; $\phi_j = \cos\left(\frac{(2j-1)\pi}{2J}\right)$; $w = \frac{1}{2}(\phi_j + 1)$.

Proof After some basic albegra calculations, Eq. 21 becomes

$$\mathrm{SEP} = \frac{a\sqrt{b}}{2\sqrt{2\pi}}\int_0^{\infty}\frac{e^{-bx/2}}{\sqrt{x}}F(x)dx. \quad (23)$$

Based on the definitions of the CDF and the outage probability, we can replace $F(x)$ in Eq. 23 with P_{out} in Eq. 16. After some mathematical transforms, we obtain the SEP of the proposed system. □

The detailed proof is represented in Appendix B.

4 Numerical results and discussion

In this section, we use the expressions in Theorem 1 and Theorem 2 to evaluate the performance of the proposed system. Furthermore, to verify the correctness of the mathematical analysis, we conduct Monte-Carlo simulations to compare the analytical results with simulation results. In our proposed system, the average SNR is defined as the ratio of the average transmission power of PB to the variance of AWGN, i.e., SNR $= P/\sigma^2$. On the other hand, we choose the average channel gains $\Omega_l = 1$ with $l = 1, 2, ..., 6$; the energy harvesting efficiency $\eta = 0.85$. The simulation results were obtained by using 10^6 channel realizations so that the simulation results can converge to the analysis results.

Figure 3 illustrates the outage probability of the proposed system versus the average SNR. We use minimum data rate

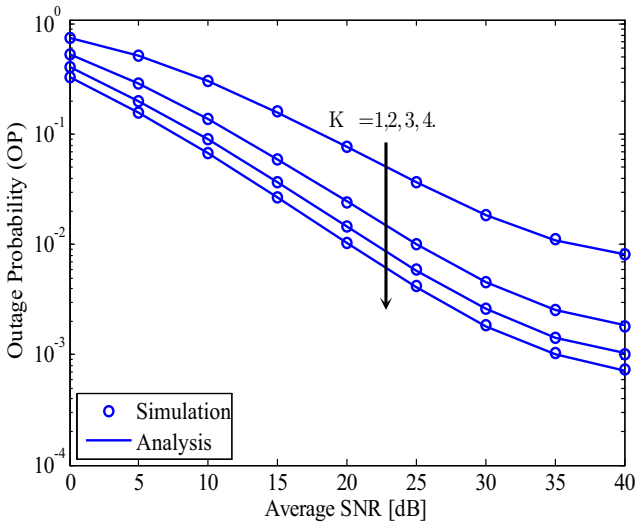

Fig. 3 The outage probability of the proposed system versus the average SNR for different number of transmission antennas of PB, $\mathcal{R} = 1$ bit/s/Hz, $\tilde{\Omega} = -30$ dB, $\alpha = 0.5$, $d_{\text{SR}} = d_{\text{RD}} = 0.5$, $\beta = 4$

$\mathcal{R} = 1$ bit/s/Hz, the SIC capability $\tilde{\Omega} = -30$ dB, the time switching ratio $\alpha = 0.5$, the distances between S and R and between R and D are $d_{\text{SR}} = d_{\text{RD}} = 0.5$ so that $d_{\text{SR}} + d_{\text{RD}} = 1$ [18, 44], the path loss exponent $\beta = 4$, and the number of transmission antennas of PB vary from 1 to 4. The analysis curves are plotted by using Eq. 16 in Theorem 1, while the symbol markers indicate Monte-Carlo simulation results. It is easy to see that the theoretical analysis is perfectly matched with the simulation. Furthermore, the outage probability is reduced when we increase the number of transmission antennas of PB. It is reasonable because when the number of transmission antennas of PB increases, the amounts of harvested energy at S and R become higher, thus reduces the outage probability. However, we can see that the reduction in the outage probability is non-linear.

Figure 4 depicts the impact of EH duration α on the outage probability of the proposed system with various SNR. We evaluate the OP with K = 3 transmission antennas at PB and four different values of SNR, i.e., SNR = 10, 20, 30, 40 dB. Other parameters are the same as those in Fig. 3. As can be seen in Fig. 4, there exists an optimal value of α, which gives the lowest OP for this system. On the other hand, this value is different for each SNR. For example, the optimal value of α is about $\alpha = 0.2$ when SNR = 40 dB and $\alpha = 0.4$ when SNR = 30 dB. When the transmission power of PB decreases, that value will increase. For example, in the case SNR = 10 dB, the optimal value is $\alpha = 0.6$. It is because when the transmission power of PB is low, S and R need more time to have enough energy for data exchange. As a result, the time duration for information transmission is decreased. In the case of the high transmission power of PB, S and R can harvest enough energy in a short time, leading

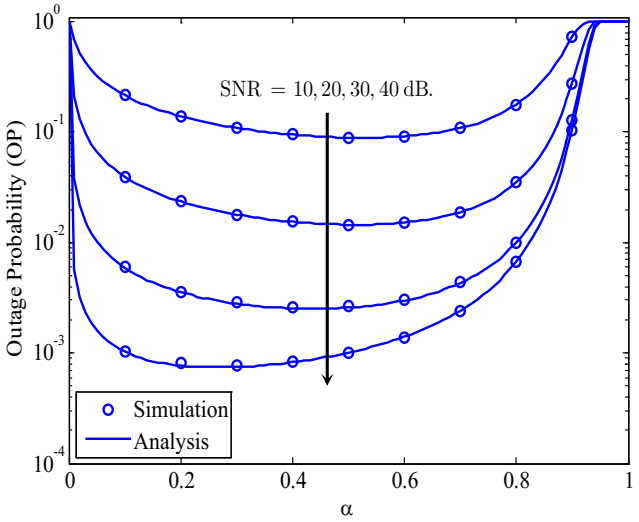

Fig. 4 The impact of EH time duration on the outage probability of the proposed system with various SNR, $\mathcal{R} = 1$ bit/s/Hz, $\tilde{\Omega} = -30$ dB, $d_{\text{SR}} = d_{\text{RD}} = 0.5$, $\beta = 4$, K = 3

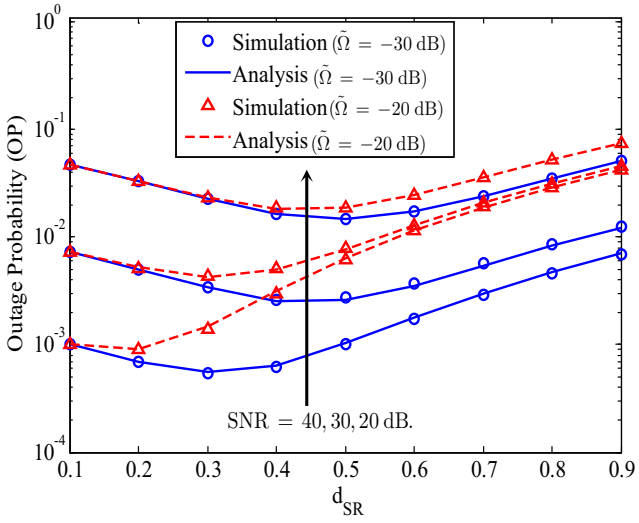

Fig. 6 The OP of the proposed system versus the distance d_{SR} with $\mathcal{R} = 1$ bit/s/Hz, $\tilde{\Omega} = -30, -20$ dB, $\alpha = 0.5$, $\beta = 4$, K = 3

to the reduction in the EH duration. Consequently, based on the transmission power of PB, we can adjust the EH time duration to improve the outage performance of the proposed system.

Figure 5 shows the impact of RSI on the outage probability of the proposed EH-FD-V2V relay system. It is easy to see that the RSI has a strong influence on the outage performance. When the RSI is small, such as $\tilde{\Omega} = -30$ dB, the OP rapidly decreases when SNR increases. However, for larger RSI, such as $\tilde{\Omega} = -20$ dB, the OP decreases slowly and reaches the outage floor at SNR = 30 dB. The outage floor is reached faster at SNR = 20 dB when $\tilde{\Omega} = -10$ dB and at SNR = 10 dB when $\tilde{\Omega} = 0$ dB. Therefore, it is

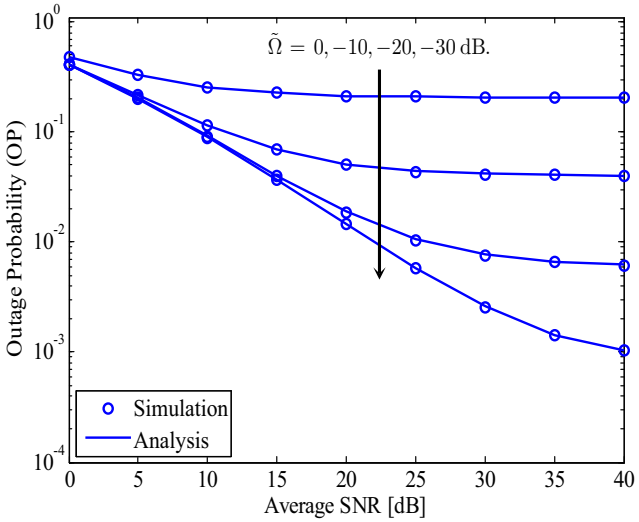

Fig. 5 The OP of the proposed EH-FD-V2V relay system under the impact of the RSI at the FD relay node with $\mathcal{R} = 1$ bit/s/Hz, $\alpha = 0.5$, $d_{\text{SR}} = d_{\text{RD}} = 0.5$, $\beta = 4$, K = 3, $\tilde{\Omega} = -30, -20, -10, 0$ dB

important to effectively apply various SIC techniques for the FD relay node so that the outage floor can be avoided.

Figure 6 investigates the impact of d_{SR} on the OP of the proposed system. We set $d_{\text{SR}} + d_{\text{RD}} = 1$ for two values of the RSI and three values of SNRs. It is obvious that when SNR increases, such as from 20 to 40 dB, the optimal value of d_{SR} which minimizes the OP decreases. For example, in the case SNR = 20 dB and $\tilde{\Omega} = -30$ dB, the OP is lowest when $d_{\text{SR}} = d_{\text{RD}} = 0.5$. However, when SNR increases to SNR = 40 dB and $\tilde{\Omega} = -30$ dB, the OP is lowest when $d_{\text{SR}} = 0.3$ and $d_{\text{RD}} = 0.7$. On the other hand, if the SIC capability and SNR increase, d_{SR} which gives the lowest OP is shorter. Particularly, in the case $\tilde{\Omega} = -20$ dB, the OP is lowest when $d_{\text{SR}} = 0.4$, $d_{\text{RD}} = 0.6$ and SNR = 20 dB and when $d_{\text{SR}} = 0.2$, $d_{\text{RD}} = 0.8$ and SNR = 40 dB. This is suitable for the proposed system because increasing SNR requires higher transmission power of the FD relay node, thus the RSI increases. From Eqs. 10 and 11, we can see that the SINR at D increases but the SINR at R does not. Therefore, to increase the SINR at R we need to reduce the distance d_{SR}.

Figure 7 illustrates the system throughput of the proposed EH-FD-V2V relay system versus the average SNR for various time switching ratio α. The system throughput is defined by $\text{T}_{\text{put}} = \mathcal{R}(1-\alpha)(1-P_{\text{out}})$, where P_{out} is given in Eq. 16. As obviously shown in Fig. 7, when the EH duration is short, i.e., α is small, the proposed system has the highest throughput. For example, when $\alpha = 0.1$ we achieve the best system throughput. More specifically, when $\alpha = 0.1$ the system throughput reaches 0.9 bit/s/Hz when SNR = 30 dB. However, when $\alpha = 0.9$, the system throughput only reaches 0.1 bit/s/Hz while the target throughput $\mathcal{R} = 1$ bit/s/Hz. Therefore, for the proposed system, we need to

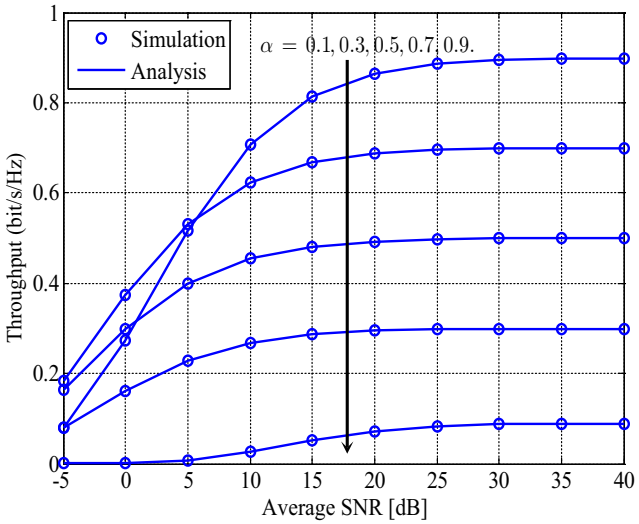

Fig. 7 The throughput of the proposed EH-FD-V2V relay system versus the average SNR for different values of α, $\mathcal{R} = 1$, $\tilde{\Omega} = -30$ dB, $d_{\mathrm{SR}} = d_{\mathrm{RD}} = 0.5$, $\beta = 4$, K = 3

reduce the EH duration to get higher throughput. Using both Figs. 4 and 7, we can choose a suitable value of α to achieve low outage probability and high system throughput. For example, we can use $\alpha = 0.3$ in high SNR region such as SNR = 30 dB to obtain OP = 0.0028 (while the lowest OP is 0.0026, Fig. 4) and the system throughput $\mathrm{T_{put}} = 0.7$ bit/s/Hz (Fig. 7).

Figure 8 plots the symbol error probability of the proposed system when BPSK ($a = 1, b = 2$) and 4QAM or QPSK ($a = 2, b = 1$) modulations are used. We consider two cases of the distances from S to R and from R to D, i.e., $d_{\mathrm{SR}} = d_{\mathrm{RD}} = 0.5$ and $d_{\mathrm{SR}} = d_{\mathrm{RD}} = 1$. In Fig. 8, the analysis curves are plotted by using Eq. 22 in

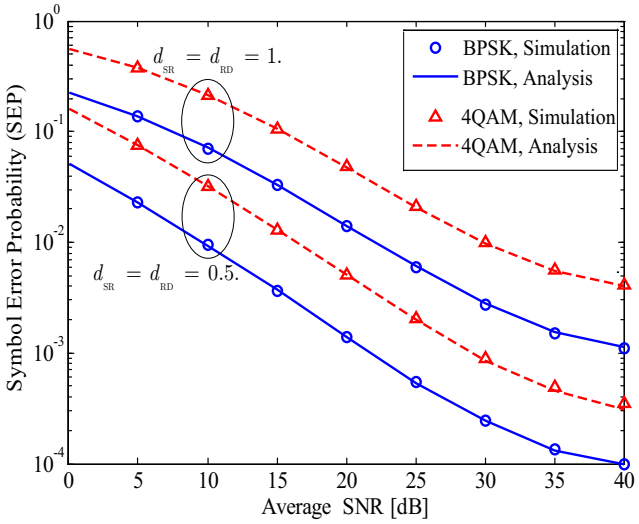

Fig. 8 The SEP of the proposed EH-FD-V2V relay system using BPSK and 4QAM/QPSK modulations with $\alpha = 0.5$, $\tilde{\Omega} = -30$ dB, K = 3, $\beta = 4$, $d_{\mathrm{SR}} = d_{\mathrm{RD}} = 0.5$, and $d_{\mathrm{SR}} = d_{\mathrm{RD}} = 1$

Theorem 2, and the symbol makers refer to Monte-Carlo simulation results. We can see that the diversity order of the proposed EH-FD-V2V relay system is one in the case $d_{\mathrm{SR}} = d_{\mathrm{RD}} = 0.5$. On the other hand, all SEPs tend towards the error floor in the high SNR regime due to the RSI of FD mode. Furthermore, the SEP of the system in the case $d_{\mathrm{SR}} = d_{\mathrm{RD}} = 1$ cannot be less than 10^{-3} even when the transmission power of PB gets higher.

5 Conclusion

Motivated by the advantages of the EH and FD techniques, in this paper, we mathematically analyze the performance of the proposed EH-FD-V2V relay system where the source and relay node harvest the energy over double Rayleigh fading channels. Specifically, we derive the exact expressions of the outage and symbol error probabilities of the proposed system. The numerical results show that the system performance in terms of the outage and symbol error probabilities is strongly impacted by the number of transmission antennas of PB, the time duration for energy harvesting, the distances between nodes, the path loss exponent, and the SIC capability of FD relay node. Moreover, for given transmission power of PB, there is an optimal value of the EH duration α, which offers the lowest OP and high system throughput. Thus, depending on the transmission power of PB, the SIC capability, and other system parameters, we can choose a suitable value of EH duration to maximize the system performance.

Appendix A

This appendix presents step-by-step derivations of the mathematical expression of the outage probability in Theorem 1. Firstly, the probability $\Pr\{\gamma_{\mathrm{R}} < x\}$ is calculated as Eq. A1.

$$\begin{aligned}\Pr\{\gamma_{\mathrm{R}} < x\} &= \Pr\left\{\frac{\eta\alpha P|h_{\mathrm{SR}}|^2}{(1-\alpha)d_{\mathrm{SR}}^{\beta}(\gamma_{\mathrm{RSI}}+\sigma^2)}\sum_{i=1}^{\mathrm{K}}|h_{i\mathrm{S}}|^2 < x\right\}\\ &= \Pr\left\{|h_{\mathrm{SR}}|^2 < \frac{(1-\alpha)d_{\mathrm{SR}}^{\beta}(\gamma_{\mathrm{RSI}}+\sigma^2)x}{\eta\alpha P\sum_{i=1}^{\mathrm{K}}|h_{i\mathrm{S}}|^2}\right\} \quad \text{(A1)}\end{aligned}$$

Due to the fact that $|h_{\mathrm{SR}}|^2 = |h_{\mathrm{SR}_1}|^2|h_{\mathrm{SR}_2}|^2$, the CDF of $|h_{\mathrm{SR}}|^2$ is computed as

$$\begin{aligned}F_{|h_{\mathrm{SR}}|^2}(x) &= \Pr(|h_{\mathrm{SR}_1}|^2|h_{\mathrm{SR}_2}|^2 < x)\\ &= \int_0^{\infty}\Pr\left(|h_{\mathrm{SR}_2}|^2 < \frac{x}{y}\right)f_{|h_{\mathrm{SR}_1}|^2}(y)dy. \quad \text{(A2)}\end{aligned}$$

From Eqs. 17 and 18, we can rewrite (A2) as

$$F_{|h_{\mathrm{SR}}|^2}(x) = 1 - \frac{1}{\Omega_3}\int_0^{\infty} \exp\left(-\frac{y}{\Omega_3} - \frac{x}{y\Omega_4}\right) dy$$
$$= 1 - \sqrt{\frac{4x}{\Omega_3\Omega_4}} K_1\left(\sqrt{\frac{4x}{\Omega_3\Omega_4}}\right). \quad \text{(A3)}$$

We can see from Eq. A3 that, the CDF of $|h_{\mathrm{SR}}|^2$ implicitly takes into account the effects of scatterers around the transmitter and the receiver which include the fluctuating amplitude and phase of signal, the Doppler shifts caused by the movement of vehicles [26].

Using Eqs. A3, 20, and A1 becomes (A4). It is also noted that, we set $\Omega_1 = \mathbb{E}\{|h_{i\mathrm{S}}|^2\}$, $\Omega_3 = \mathbb{E}\{|h_{\mathrm{SR}_1}|^2\}$ and $\Omega_4 = \mathbb{E}\{|h_{\mathrm{SR}_2}|^2\}$ in Eq. A4.

$$\Pr\{\gamma_{\mathrm{R}} < x\} = \int_0^{\infty}\left[1 - \sqrt{\frac{4(1-\alpha)d_{\mathrm{SR}}^{\beta}(\gamma_{\mathrm{RSI}}+\sigma^2)x}{\Omega_3\Omega_4\eta\alpha P y}} K_1\left(\sqrt{\frac{4(1-\alpha)d_{\mathrm{SR}}^{\beta}(\gamma_{\mathrm{RSI}}+\sigma^2)x}{\Omega_3\Omega_4\eta\alpha P y}}\right)\right]\frac{y^{\mathrm{K}-1}}{\Omega_1^{\mathrm{K}}\Gamma(\mathrm{K})}\exp\left(-\frac{y}{\Omega_1}\right)$$
$$= \int_0^{\infty}\left[1 - \sqrt{\frac{Ax}{y}} K_1\left(\sqrt{\frac{Ax}{y}}\right)\right]\frac{y^{\mathrm{K}-1}}{\Omega_1^{\mathrm{K}}\Gamma(\mathrm{K})}\exp\left(-\frac{y}{\Omega_1}\right)$$
$$= \frac{1}{\Omega_1^{\mathrm{K}}\Gamma(\mathrm{K})}\left[\int_0^{\infty} y^{\mathrm{K}-1}\exp\left(-\frac{y}{\Omega_1}\right)dy - \sqrt{Ax}\int_0^{\infty} K_1\left(\sqrt{\frac{Ax}{y}}\right) y^{\mathrm{K}-\frac{3}{2}}\exp\left(-\frac{y}{\Omega_1}\right)dy\right]. \quad \text{(A4)}$$

For the first integral in Eq. A4, we apply [42, 3.351.3] to have

$$\int_0^{\infty} y^{\mathrm{K}-1}\exp\left(-\frac{y}{\Omega_1}\right)dy = \Omega_1^{\mathrm{K}}\Gamma(\mathrm{K}). \quad \text{(A5)}$$

For the second integral in Eq. A4, we set $t = \exp\left(-\frac{y}{\Omega_1}\right)$. After some algebra calculations, we obtain the following integral

$$\int_0^{\infty} K_1\left(\sqrt{\frac{Ax}{y}}\right) y^{\mathrm{K}-\frac{3}{2}}\exp\left(-\frac{y}{\Omega_1}\right)dy$$
$$= \Omega_1\int_0^{1} K_1\left(\sqrt{\frac{Ax}{-\Omega_1\ln t}}\right)(-\Omega_1\ln t)^{\mathrm{K}-\frac{3}{2}}dt. \quad \text{(A6)}$$

Applying the Gaussian-Chebyshev quadrature method in [45], Eq. A6 becomes

$$\Omega_1\int_0^{1} K_1\left(\sqrt{\frac{Ax}{-\Omega_1\ln t}}\right)(-\Omega_1\ln t)^{\mathrm{K}-\frac{3}{2}}dt$$
$$= \frac{\Omega_1\pi}{2M}\sum_{m=1}^{M}\sqrt{1-\phi_m^2}\,K_1\left(\sqrt{\frac{Ax}{-\Omega_1\ln u}}\right)(-\Omega_1\ln u)^{\mathrm{K}-\frac{3}{2}}. \quad \text{(A7)}$$

Substituting Eqs. A5 and A7 into Eq. A4, we get (A8).

$$\Pr\{\gamma_{\mathrm{R}} < x\} = \frac{1}{\Omega_1^{\mathrm{K}}\Gamma(\mathrm{K})}\left[\Omega_1^{\mathrm{K}}\Gamma(\mathrm{K}) - \sqrt{Ax}\frac{\Omega_1\pi}{2M}\sum_{m=1}^{M}\sqrt{1-\phi_m^2}\right.$$
$$\left.\times K_1\left(\sqrt{\frac{Ax}{-\Omega_1\ln u}}\right)(-\Omega_1\ln u)^{\mathrm{K}-\frac{3}{2}}\right]$$
$$= 1 - \frac{\pi\sqrt{Ax}}{2M(\Omega_1)^{\mathrm{K}-1}\Gamma(\mathrm{K})}\sum_{m=1}^{M}\sqrt{1-\phi_m^2}$$
$$\times K_1\left(\sqrt{\frac{Ax}{-\Omega_1\ln u}}\right)(-\Omega_1\ln u)^{\mathrm{K}-\frac{3}{2}} \quad \text{(A8)}$$

By doing the same calculations as for $\Pr\{\gamma_{\mathrm{R}} < x\}$ for $\Pr\{\gamma_{\mathrm{D}} < x\}$, we have (A9).

$$\Pr\{\gamma_{\mathrm{D}} < x\} = \Pr\left\{\frac{\eta\alpha P|h_{\mathrm{RD}}|^2}{(1-\alpha)d_{\mathrm{RD}}^{\beta}\sigma^2}\sum_{i=1}^{\mathrm{K}}|h_{i\mathrm{R}}|^2 < x\right\}$$
$$= \Pr\left\{|h_{\mathrm{RD}}|^2 < \frac{(1-\alpha)d_{\mathrm{RD}}^{\beta}\sigma^2 x}{\eta\alpha P\sum_{i=1}^{\mathrm{K}}|h_{i\mathrm{R}}|^2}\right\}$$
$$= 1 - \frac{\pi\sqrt{Bx}}{2N(\Omega_2)^{\mathrm{K}-1}\Gamma(\mathrm{K})}\sum_{n=1}^{N}\sqrt{1-\phi_n^2}$$
$$\times K_1\left(\sqrt{\frac{Bx}{-\Omega_2\ln v}}\right)(-\Omega_2\ln v)^{\mathrm{K}-\frac{3}{2}}. \quad \text{(A9)}$$

Then, plugging Eqs. A8 and A9 into Eq. 15, we obtain (16) in Theorem 1 which is the closed-form expression of the outage probability of the proposed system. The proof is complete.

Appendix B

In this section, we provide the detailed derivations of Eq. 22 in Theorem 2.

Replacing $F(x)$ in Eq. 23 with P_{out} in Eq. 16, we obtain (B1).

$$\begin{aligned}\text{SEP} &= \frac{a\sqrt{b}}{2\sqrt{2\pi}}\int_0^\infty \frac{e^{-bx/2}}{\sqrt{x}}\Bigg[1-\frac{\pi^2\sqrt{AB}x}{4MN(\Omega_1\Omega_2)^{\text{K}-1}\Gamma^2(\text{K})}\\ &\quad\times\sum_{m=1}^{M}\sum_{n=1}^{N}\sqrt{(1-\phi_m^2)(1-\phi_n^2)}K_1\left(\sqrt{\frac{Ax}{-\Omega_1\ln u}}\right)\\ &\quad\times K_1\left(\sqrt{\frac{Bx}{-\Omega_2\ln v}}\right)(\Omega_1\Omega_2\ln u\ln v)^{\text{K}-\frac{3}{2}}\Bigg]dx\\ &= \frac{a\sqrt{b}}{2\sqrt{2\pi}}\Bigg[\int_0^\infty\frac{e^{-bx/2}}{\sqrt{x}}dx-\frac{\pi^2\sqrt{AB}(\Omega_1\Omega_2\ln u\ln v)^{\text{K}-\frac{3}{2}}}{4MN(\Omega_1\Omega_2)^{\text{K}-1}\Gamma^2(\text{K})}\\ &\quad\times\sum_{m=1}^{M}\sum_{n=1}^{N}\sqrt{(1-\phi_m^2)(1-\phi_n^2)}\\ &\quad\times\int_0^\infty x^{\frac{1}{2}}e^{-bx/2}K_1\left(\sqrt{\frac{Ax}{-\Omega_1\ln u}}\right)K_1\left(\sqrt{\frac{Bx}{-\Omega_2\ln v}}\right)dx\Bigg].\end{aligned}\tag{B1}$$

For the first integral in Eq. B1, we use [42, 3.361.2] to solve it, i.e.,

$$\int_0^\infty\frac{e^{-bx/2}}{\sqrt{x}}dx=\sqrt{\frac{2\pi}{b}}.\tag{B2}$$

For the second integral in Eq. B1, we set $z=e^{-bx/2}$. After some mathematical calculations, we get (B3).

$$\begin{aligned}&\int_0^\infty x^{\frac{1}{2}}e^{-bx/2}K_1\left(\sqrt{\frac{Ax}{-\Omega_1\ln u}}\right)K_1\left(\sqrt{\frac{Bx}{-\Omega_2\ln v}}\right)\\ &\quad dx=\frac{2}{b}\int_0^1\sqrt{\frac{-2\ln z}{b}}K_1\left(\sqrt{\frac{2A\ln z}{b\Omega_1\ln u}}\right)K_1\left(\sqrt{\frac{2B\ln z}{b\Omega_2\ln v}}\right)dz.\end{aligned}\tag{B3}$$

Due to the complexity of the integral in Eq. B3, it is hard to find the closed-form expression for this integral. Therefore, we use the Gaussian-Chebyshev quadrature method in [45] to solve this integral. After that, we have (B4).

$$\begin{aligned}&\frac{2}{b}\int_0^1\sqrt{\frac{-2\ln z}{b}}K_1\left(\sqrt{\frac{2A\ln z}{b\Omega_1\ln u}}\right)K_1\left(\sqrt{\frac{2B\ln z}{b\Omega_2\ln v}}\right)dz=\frac{\pi}{Jb}\\ &\quad\times\sum_{j=1}^{J}\sqrt{1-\phi_j^2}\sqrt{\frac{-2\ln w}{b}}K_1\left(\sqrt{\frac{2A\ln w}{b\Omega_1\ln u}}\right)K_1\left(\sqrt{\frac{2B\ln w}{b\Omega_2\ln v}}\right).\end{aligned}\tag{B4}$$

Substituting Eqs. B2 and B4 into Eq. B1, we obtain (22) in Theorem 2 which is the closed-form expression of the SER of the proposed system. The proof is complete.

References

1. Gazestani AH, Ghorashi SA, Mousavinasab B, Shikh-Bahaei M (2019) A survey on implementation and applications of full duplex wireless communications. Physical Communication 34:121–134
2. Wang CX, Bian J, Sun J, Zhang W, Zhang M (2018) A survey of 5G channel measurements and models. IEEE Communications Surveys & Tutorials 20(4):3142–3168
3. Zhang D, Liu Y, Dai L, Bashir AK, Nallanathan A, Shim B (2019) Performance analysis of FD-NOMA-based decentralized V2X systems. IEEE Transactions on Communications 67(7):5024–5036
4. Kolodziej KE, Perry BT, Herd JS (2019) In-band full-duplex technology: techniques and systems survey. IEEE Transactions on Microwave Theory and Techniques 67(7):3025–3041
5. Nguyen NP, Ngo HQ, Duong TQ, Tuan HD, da Costa DB (2017) Full-duplex cyber-weapon with massive arrays. IEEE Transactions on Communications 65(12):5544–5558
6. Zhang T, Cai Y, Huang Y, Duong TQ, Yang W (2017) Secure full-duplex spectrum-sharing wiretap networks with different antenna reception schemes. IEEE Trans Commun 65(1):335–346
7. Deng Y, Kim KJ, Duong TQ, Elkashlan M, Karagiannidis GK, Nallanathan A (2016) Full-duplex spectrum sharing in cooperative single carrier systems. IEEE Trans Cognitive Commun Network 2(1):68–82
8. Nguyen NP, Kundu C, Ngo HQ, Duong TQ, Canberk B (2016) Secure full-duplex small-cell networks in a spectrum sharing environment. IEEE Access 4:3087–3099
9. Doan XT, Nguyen NP, Yin C, Da Costa DB, Duong TQ (2017) Cognitive full-duplex relay networks under the peak interference power constraint of multiple primary users. EURASIP J Wirel Commun Netw 2017(1):1–10
10. Nguyen BC, Hoang TM, Tran PT (2019) Performance analysis of full-duplex decode-and-forward relay system with energy harvesting over Nakagami-*m* fading channels. AEU-International Journal of Electronics and Communications 98:114–122
11. Ba CaoNguyen, Thang NguyenNhu, Tran XuanNam, Dung LT (2020) Impacts of imperfect channel state information, transceiver hardware, and self-interference cancellation on the performance of full-duplex MIMO relay system. Sensors 20(6):1671
12. Bharadia D, McMilin E, Katti S (2013) Full duplex radios. In: ACM SIGCOMM computer communication review, vol 43. ACM, pp 375–386

13. Li X, Tepedelenlioglu C, Senol H (2017) Channel estimation for residual self-interference in full duplex amplify-and-forward two-way relays. IEEE Transactions on Wireless Communications 16(8):4970–4983
14. Antonio-Rodríguez E, López-Valcarce R, Riihonen T, Werner S, Wichman R (2013) Adaptive self-interference cancellation in wideband full-duplex decode-and-forward MIMO relays. In: 2013 IEEE 14th workshop on signal processing advances in wireless communications (SPAWC). IEEE, pp 370–374
15. Hoang TM, Tan NT, Cao NB, Dung LT (2017) Outage probability of MIMO relaying full-duplex system with wireless information and power transfer. In: 2017 conference on information and communication technology (CICT), pp 1–6
16. Dung LT, Nguyen BC, Hoang TM, Choi SG (2018) Full-duplex relay system with energy harvesting: outage and symbol error probabilities. In: 2018 international conference on advanced technologies for communications (ATC). IEEE, pp 360–365
17. Li S, Kun Y, Zhou M, Wu J, Song L, Li Y, Li H (2017) Full-duplex amplify-and-forward relaying: power and location optimization. IEEE Transactions on Vehicular Technology 66(9):8458–8468
18. Li C, Chen Z, Wang Y, Yao Y, Xia B (2017) Outage analysis of the full-duplex decode-and-forward two-way relay system. IEEE Transactions on Vehicular Technology 66(5):4073–4086
19. Van Nguyen L, Nguyen BC, Tran XN, Dung LT (2020) Transmit antenna selection for full-duplex spatial modulation multiple-input multiple-output system. IEEE Systems Journal 14(4):4777–4785
20. Campolo C, Molinaro A, Berthet AO, Vinel A (2017) Full-duplex radios for vehicular communications. IEEE Communications Magazine 55(6):182–189
21. Chen Y, Wang L, Ai Y, Jiao B, Hanzo L (2017) Performance analysis of NOMA-SM in vehicle-to-vehicle massive MIMO channels. IEEE Journal on Selected Areas in Communications 35(12):2653–2666
22. Mao CX, Gao S, Wang Y (2018) Dual-band full-duplex tx/rx antennas for vehicular communications. IEEE Transactions on Vehicular Technology 67(5):4059–4070
23. Yang M, Jeon SW, Kim DK (2018) Interference management for in-band full-duplex vehicular access networks. IEEE Transactions on Vehicular Technology 67(2):1820–1824
24. Nguyen KK, Duong TQ, Vien NA, Le-Khac NA, Nguyen LD (2019) Distributed deep deterministic policy gradient for power allocation control in D2D-based V2V communications. IEEE Access 7:164533–164543
25. Ai Y, Cheffena M, Mathur A, Lei H (2018) On physical layer security of double rayleigh fading channels for vehicular communications. IEEE Wireless Communications Letters 7(6):1038–1041
26. Kovacs IZ, Eggers PCF, Olesen K, Petersen LG (2002) Investigations of outdoor-to-indoor mobile-to-mobile radio communication channels. In: Proceedings IEEE 56th vehicular technology conference. IEEE, pp 430–434
27. Zhong C, Suraweera HA, Zheng G, Krikidis I, Zhang Z (2014) Wireless information and power transfer with full duplex relaying. IEEE Transactions on Communications 62(10):3447–3461
28. Tam HHM, Tuan HD, Nasir AA, Duong TQ, Poor HV (2017) MIMO energy harvesting in full-duplex multi-user networks. IEEE Trans Wirel Commun 16(5):3282–3297
29. Nguyen VD, Duong TQ, Tuan HD, Shin OS, Poor HV (2017) Spectral and energy efficiencies in full-duplex wireless information and power transfer. IEEE Trans Commun 65(5):2220–2233
30. Hoang TM, El Shafie A, Da Costa DB, Duong TQ, Tuan HD, Marshall A (2020) Security and energy harvesting for MIMO-OFDM networks. IEEE Trans Commun 68(4):2593–2606
31. Nasir AA, Hoang TD, Duong TQ, Hanzo L (2020) Transmitter-side wireless information- and power-transfer in massive MIMO systems. IEEE Transactions on Vehicular Technology 9(2):2322–2326
32. Zhou X, Zhang R, Ho CK (2013) Wireless information and power transfer: architecture design and rate-energy tradeoff. IEEE Transactions on Communications 61(11):4754–4767
33. Yang K, Cui H, Song L, Li Y (2015) Efficient full-duplex relaying with joint antenna-relay selection and self-interference suppression. IEEE Transactions on Wireless Communications 14(7):3991–4005
34. Nguyen BC, Tran XN (2019) Performance analysis of full-duplex amplify-and-forward relay system with hardware impairments and imperfect self-interference cancellation. Wireless Communications and Mobile Computing 29(Article ID 4946298):1–10
35. Nguyen LV, Nguyen BC, Tran XN (2019) Closed-form expression for the symbol error probability in full-duplex spatial modulation relay system and its application in optimal power allocation. Sensors 19(24):5390
36. Nguyen BC, Tran XN, Tran DT, Dung LT (2019) Full-duplex amplify-and-forward relay system with direct link: performance analysis and optimization. Physical Communication 37:100888
37. Hong S, Brand J, Choi JI, Jain M, Mehlman J, Katti S, Levis P (2014) Applications of self-interference cancellation in 5G and beyond. IEEE Communications Magazine 52(2):114–121
38. Lu X, Wang P, Niyato D, Kim DI, Han Z (2015) Wireless networks with RF energy harvesting: a contemporary survey. IEEE Communications Surveys & Tutorials 17(2):757–789
39. Sabharwal A, Schniter P, Guo D, Bliss DW, Rangarajan S, Wichman R (2014) In-band full-duplex wireless: challenges and opportunities. IEEE Journal on Selected Areas in Communications 32(9):1637–1652
40. Goldsmith A (2005) Wireless communications. Cambridge University Press, Cambridge
41. Leon-Garcia A, Leon-Garcia A (2008) Probability, statistics, and random processes for electrical engineering, 3rd edn. Pearson/Prentice Hall, Upper Saddle River
42. Jeffrey A, Zwillinger D (2007) Table of integrals, series, and products. Academic Press, Cambridge, Massachusetts
43. Shankar PM (2017) Fading and shadowing in wireless systems. Springer, Berlin
44. Duy TT, Alexandropoulos GC, Tung VT, Son VN, Duong TQ (2016) Outage performance of cognitive cooperative networks with relay selection over double-rayleigh fading channels. IET Communications 10(1):57–64
45. Abramowitz M, Stegun IA (1972) Handbook of mathematical functions with formulas, graphs, and mathematical tables, vol 9. Dover, New York